

Muon $g-2$ with overlap valence fermion



(χ QCD Collaboration)

Gen Wang,^{1,2,*} Terrence Draper,² Keh-Fei Liu,² and Yi-Bo Yang^{3,4,5,6,†}

¹*Aix-Marseille Université, Université de Toulon, CNRS, CPT, Marseille, France*

²*Department of Physics and Astronomy, University of Kentucky, Lexington, KY 40506, USA*

³*CAS Key Laboratory of Theoretical Physics, Institute of Theoretical Physics, Chinese Academy of Sciences, Beijing 100190, China*

⁴*University of Chinese Academy of Sciences, School of Physical Sciences, Beijing 100049, China*

⁵*School of Fundamental Physics and Mathematical Sciences, Hangzhou Institute for Advanced Study, UCAS, Hangzhou 310024, China*

⁶*International Centre for Theoretical Physics Asia-Pacific, Beijing/Hangzhou, China*

We present a lattice calculation of the leading order (LO) hadronic vacuum polarization (HVP) contribution to the muon anomalous magnetic moment for the connected light and strange quarks, $a_{\text{con},l/s}^{\text{W}}$ in the widely used window $t_0 = 0.4$ fm, $t_1 = 1.0$ fm, $\Delta = 0.15$ fm, and also of $a_{\text{con},l/s}^{\text{S}}$ in the short distance region. We use the overlap fermion on 4 physical-point ensembles. Two 2+1 flavors ensembles use the domain wall fermion (DWF) and Iwasaki gauge actions at $a = 0.084$ and 0.114 fm, and two 2+1+1 flavors ensembles use the highly-improved-staggered-quark (HISQ) and Symanzik gauge actions at $a = 0.088$ and 0.121 fm. They have incorporated infinite volume corrections from 3 additional DWF ensembles at $L = 4.8, 6.4$ and 9.6 fm and physical pion mass. For the $a_{\text{con},l}^{\text{W}}$, we find that our results on the two smaller lattice spacings are consistent with those using the unitary setup, but those at the two coarser lattice spacings have obviously small differences compared to the unitary ones.

I. INTRODUCTION

The anomalous magnetic moment of the muon ($a_\mu \equiv (g_\mu - 2)/2$) is one of the crucial benchmarks to verify the correctness of the standard model. The current analysis of the Fermilab experiment [1, 2] is consistent with the previous BNL E821 [3] result with comparable precision, and the Fermilab experiment is planned to reduce the uncertainty by a factor of 4. Those results are higher than the current standard model predictions [4] using phenomenological estimates by around 4σ , and so have attracted much theoretical interest about possible new physics.

But such a deviation is very sensitive to the theoretical prediction of the strong interaction contribution to a_μ , especially the leading order hadronic vacuum polarization (LO-HVP) contribution, $a_\mu^{\text{LO-HVP}}$. The most recent determinations from the hadronic R -ratio, a dispersion integral over hadronic cross section ratio $\sigma(e^+e^- \rightarrow \text{hadrons})/\sigma(e^+e^- \rightarrow \mu^+\mu^-)$, are $\bar{a} \equiv a_\mu^{\text{LO-HVP}} \times 10^{10} = 693.9(4.0)$ [5] and 692.8(2.4) [6], while that required for no new physics is 718(4) [1–4]. Comparing to $a_\mu^{\text{LO-HVP}}$, the electron mass suppresses $a_e^{\text{LO-HVP}}$, the corresponding quantity for the electron, by a factor of $(m_e/m_\mu)^2 \sim$

10^{-4} , and so the theoretical uncertainty of HVP will not affect the agreement between the current theoretical and experimental determinations of a_e .

$a_\mu^{\text{LO-HVP}}$ can be obtained using first-principles Lattice QCD calculations, which avoid the possible phenomenological uncertainty from the R -ratio determination. There are a few recent Lattice QCD results [7–12], and the most precise one [12] obtains $\bar{a} = 707.5(5.5)$ and agrees with the “no new physics” requirement within 1.5σ . A recent study [13] suggests that the so-called “window” value [8] of a_μ , which picks the contribution around the ρ meson pole, is sensitive to the discretized fermion action used by the \bar{a}_μ calculation. In this work, we will calculate the window value of a_μ using the overlap valence fermion action on ensembles with either the Domain Wall fermion (DWF) sea or HISQ sea, to study the fermion action dependence. We will also examine the lattice spacing dependence in these cases.

The numerical setups of this work are collected in Sec. II and Sec. III presents our results with their statistical and systematic uncertainties. The summary and extended discussions are given in Sec. IV.

II. NUMERICAL SETUP

One can calculate $a_\mu^{\text{LO-HVP}}$ with the following expression,

* gen.wang@univ-amu.fr

† ybyang@itp.ac.cn

$$a_\mu^{\text{LO-HVP}} = 4\alpha^2 \int_0^\infty \frac{dq^2}{m_\mu^2} f\left(\frac{q^2}{m_\mu^2}\right) (\Pi(q^2) - \Pi(0)), \quad (1)$$

$$f(r) = \frac{Z^3(r)(1 - \sqrt{r}Z(r))}{\sqrt{r}(1 + Z^2(r))}, \quad Z(r) = \frac{\sqrt{r+4} - \sqrt{r}}{2},$$

$\alpha = \frac{e^2}{4\pi} \sim 1/137$ is the fine structure constant, m_μ is the muon mass, the HVP $\Pi(q^2)$ can be obtained from the Fourier transform of the vector current two-point function in Euclidean space-time,

$$\Pi^{\mu\nu}(q) = \int d^4x e^{iqx} \langle j_\mu(x) j_\nu(0) \rangle = \Pi(q^2)(q^2 \delta_{\mu\nu} - q_\mu q_\nu), \quad (2)$$

and the electromagnetic current $j_\mu = \sum_f Q_f \bar{\psi}_f \gamma_\mu \psi_f$ is summed over all the quark flavors $f = u, d, s, c, \dots$ with their electric charge Q_f in units of the electron charge e . The factor Z has the properties $Z(0) = 1$ and $Z(r) \propto 1/\sqrt{r}$ at $r \rightarrow \infty$, which ensures that the major contribution in the q^2 integration comes from the small q^2 region.

One can select the momentum q to be along the temporal direction to simplify the expression of $\Pi(q^2)$ to

$$\Pi(q^2) = \int dt \frac{\cos(tq)}{q^2} C(t), \quad (3)$$

where $C(t) \equiv \frac{1}{3} \sum_i \langle \int d^3x j_i(\vec{x}, t) j_i(\vec{0}, 0) \rangle$. This definition includes the $1/q^2$ divergence, but then the subtracted $\Pi(q^2)$ [14] is

$$\Pi(q^2) - \Pi(0) = \int dt \left[\frac{\cos(tq) - 1}{q^2} + \frac{1}{2} t^2 \right] C(t). \quad (4)$$

One can show that $\Pi(q^2) \propto 1/M^2$ if $C(t) \propto e^{-Mt}$ and then $a_\mu^{\text{HVP}} \propto m_\mu^2/M^2$ if $C(t)$ is dominated by a single state with mass $M \gg m_\mu$, and then the heavy quark contribution to a_μ^{HVP} is also suppressed by $1/m_Q^2$.

Eventually one can rewrite $a_\mu^{\text{LO-HVP}}$ in terms of $C(t)$ and the weight function $w(t)$,

$$a_\mu^{\text{LO-HVP}} = \int dt \omega(t) C(t),$$

$$\omega(t) = 4\alpha^2 \int_0^\infty \frac{dq^2}{m_\mu^2} f\left(\frac{q^2}{m_\mu^2}\right) \left[\frac{\cos(tq) - 1}{q^2} + \frac{1}{2} t^2 \right]. \quad (5)$$

On the lattice, one would use the original $w(t)$ or replace $w(t)$ by its lattice version [8],

$$\hat{\omega}(t) = 4\alpha^2 \int_0^\infty \frac{dq^2}{m_\mu^2} f\left(\frac{q^2}{m_\mu^2}\right) \left[\frac{\cos(tq) - 1}{\left[\frac{2}{a} \sin\left(\frac{qa}{2}\right)\right]^2} + \frac{1}{2} t^2 \right], \quad (6)$$

and sum t over all the discretized time slices $(-\frac{Ta}{2}, \frac{Ta}{2})$:

$$a_\mu^{\text{LO-HVP}, \omega} = \left[\sum \omega(t) C^{\text{lat}}(t, a) \right] \Big|_{a \rightarrow 0, T \rightarrow \infty}, \quad (7)$$

$$a_\mu^{\text{LO-HVP}, \hat{\omega}} = \left[\sum \hat{\omega}(t) C^{\text{lat}}(t, a) \right] \Big|_{a \rightarrow 0, T \rightarrow \infty}, \quad (8)$$

to obtain the final prediction of $a_\mu^{\text{LO-HVP}}$, where a is the lattice spacing, T is the dimensionless number of lattice sites along the temporal direction, and $C^{\text{lat}}(t, a) = a \{ C(t) + \mathcal{O}(a^2) \}$ is the correlation function on the lattice. Based on numerical calculation, changing the upper limit of the integral in Eq. 6 to a finite constant, such as $(\pi/a)^2$, changes the value of the integral by less than 0.005%, which is much smaller than our other uncertainties. Also, Ref. [7] suggests that the correction is about 0.02%, by introducing an integral cut-off $Q_{\text{max}}^2 = 3 \text{ GeV}^2$ in Eq. 6, which is also much smaller than all our total uncertainties.

In the practical calculation on the ensemble with 2 degenerate light flavors, $C(t)$ can be decomposed into several pieces [8],

$$C(t) = \frac{5}{9} C^{\text{con}}(t; m_l) + \frac{1}{9} C^{\text{con}}(t; m_s) + \frac{4}{9} C^{\text{con}}(t; m_c) \\ + C^{\text{dis}}(t) + \alpha C^{\text{QED}}(t) + \Delta m C^{\text{SIB}}(t) \\ + \mathcal{O}(\alpha^2, \alpha \Delta m, \Delta m^2), \quad (9)$$

where $m_l = (m_d + m_u)/2$ is the iso-symmetric light quark mass, $m_{s,c}$ are the strange and charm quark masses respectively, $C^{\text{con}}(t; m_f) = C^{\text{con}}(t, S(\vec{x} = \vec{0}, t_0 = 0; m_f))$,

$$C^{\text{con}}(t, S(\vec{x}_0, t_0; m_f)) = \frac{1}{3} \sum_i \langle \{ \int d^3x \text{Tr}[\gamma_i \gamma_5 \\ S^\dagger(\vec{x}, t + t_0; \vec{x}_0, t_0; m_f) \gamma_5 \gamma_i \\ S(\vec{x}, t + t_0; \vec{x}_0, t_0; m_f)] \} \rangle \quad (10)$$

is the connected correlation function with the quark propagator $S(m) \equiv 1/(D + m)$, C^{dis} is the contribution from the disconnected quark diagram, C^{QED} is the leading order QED correction which can be accessed from the 4-point correlation function with an infinite-volume photon [15] (the next order contribution is negligible for the precision required by a_μ), and C^{SIB} is the strong isospin breaking (SIB) effect which is proportional to $(m_d - m_u)/2$.

In this work, we use the overlap fermion on several gauge ensembles with 1-step HYP smearing to calculate a_μ^{W} . The ensembles include the 2+1 flavor DWF ensembles with the Iwasaki gauge action from the RBC/UQCD collaboration [16–18] and the 2+1+1 flavor HISQ ensemble with the Symanzik gauge action from the MILC collaboration [19].

The overlap fermion action uses a matrix sign function $\epsilon(H_w) = \frac{H_w}{\sqrt{H_w^2}}$ of the hermitian Wilson Dirac operator $H_w(-M_0) = \gamma_5 D_w(-M_0)$ to construct

$$D_{\text{ov}} = M_0 \left(1 + \gamma_5 \epsilon(H_w(-M_0)) \right), \quad (11)$$

which was proposed in Ref. [20, 21] as a discretized fermion operator satisfying the Ginsburg-Wilson relation $D_{\text{ov}} \gamma_5 + \gamma_5 D_{\text{ov}} = \frac{a}{M_0} D_{\text{ov}} \gamma_5 D_{\text{ov}}$ [22], where D_w is the Wilson Dirac operator with a negative mass such as

$M_0 = 1.5$. The DWF action can be considered as an approximation of the overlap fermion action using a slightly inaccurate $\epsilon(x)$, and the HISQ action [23] is a modified version of the staggered fermion action which is much cheaper than either DWF or overlap but which suffers from the taste mixing effect (see Ref. [13], for example).

Using the overlap fermion action for the valence quark allows us to implement low-mode substitution [24, 25] to improve the signal based on the low-lying eigenvectors of D_c ,

$$C^{\text{con,LMS}}(t) = \frac{1}{N_{\text{src}}N_g^3} \sum_i \{C^{\text{con}}(t, S^{\text{grid}}(\vec{x}_i, t_i)) - C^{\text{con}}(t, S_L^{\text{grid}}(\vec{x}_i, t_i))\} + \frac{1}{L^3T} \sum_{\vec{x}_0, t_0} C^{\text{con}}(t, S_L(\vec{x}_0, t_0)), \quad (12)$$

where $S^{\text{grid}}(\vec{x}_i, t_i) = \sum_{y \in \text{grid}} S(\vec{x}, t + t_0; \vec{x}_i + \vec{y}, t_i)$ is the quark propagator using a grid source with N_g points at each spacial dimension, N_{src} is the number of S^{grid} located at different origins (\vec{x}_i, t_i) , $S_L(m) \equiv \sum_{|\lambda| < \lambda_c} \frac{1}{\lambda + m} v_\lambda v_\lambda^\dagger$, v_λ satisfies $D_c v_\lambda = \lambda v_\lambda$ and $\lambda_c \sim 200$ MeV is the upper bound of the eigenvalue λ . The source point \vec{x}_0, t_0 loops over the whole lattice volume to have full statistics for the low-mode parts. The information of the gauge ensembles, grid source parameters and λ_c are listed in Table I.

TABLE I. Information of the ensembles, grid sources and λ_c used in this calculation, including the DWF+Iwasaki ensembles 48I and 64I [17, 18] and also the HISQ+Symanzik ensembles a12m130 and a09m130 [19] with the lattice spacings from Ref. [13]. Three DWF+Iwasaki+DSDR ensembles 24D/32D/48D [16, 18] are used to estimate the finite-volume effect, and four HISQ+Symanzik ensembles a04m310/a06m310/a09m310/a12m310 [19] with the lattice spacings from Ref. [26] are used to study the continuum extrapolation. The pion mass m_π and upper bound λ_c of the eigenvalues are in unit of MeV.

Symbol	$L^3 \times T$	a (fm)	m_π	N_{cfg}	N_{src}	N_g	λ_c
48I	$48^3 \times 96$	0.11406(26)	139	100	12	4	234
64I	$64^3 \times 128$	0.08365(25)	139	92	8	4	187
a12m130	$48^3 \times 64$	0.12121(64)	131	23	8	4	180
a09m130	$64^3 \times 96$	0.08786(47)	128	22	8	4	200
a12m310	$24^3 \times 64$	0.12129(89)	305	54	16	1	224
a09m310	$32^3 \times 96$	0.08821(71)	313	39	16	1	195
a06m310	$48^3 \times 144$	0.05740(50)	319	32	8	1	243
a04m310	$64^3 \times 192$	0.04250(40)	310	54	2	1	167
24D	$24^3 \times 64$	0.1940(19)	141	232	8	2	263
32D	$32^3 \times 64$	0.1940(19)	141	134	8	4	230
48D	$48^3 \times 64$	0.1940(19)	141	47	8	6	116

III. RESULTS AND SYSTEMATICS

The window method proposed in Ref. [8, 14] allows a more precise prediction to combine the ‘‘window’’ value

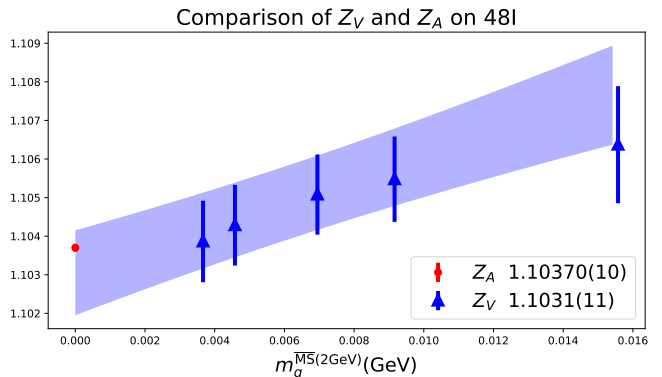


FIG. 1. Comparison of the axial normalization constant and the vector normalization constant for the local vector current on 48I. The blue band is a linear fit of the vector normalization constant at various quark masses m_q .

of $a_\mu^{\text{LO-HYP}}$ using the $C(t)$ from lattice QCD

$$a_\mu^{\text{W}} = \int dt w^{\text{W}}(t) \omega(t) C(t), \quad (13)$$

$$w^{\text{W}}(t) \equiv \theta(t, t_0, \Delta) - \theta(t, t_1, \Delta), \quad (14)$$

$$\theta(t, t', \Delta) \equiv \frac{1}{2} (1 + \tanh[(t - t')/\Delta]), \quad (15)$$

with the remaining parts

$$a_\mu^{\text{etc.}} = a_\mu^{\text{S}} + a_\mu^{\text{L}},$$

$$a_\mu^{\text{S}} = \int dt \omega(t) C(t) w^{\text{S}}(t), \quad w^{\text{S}}(t) \equiv 1 - \theta(t, t_0, \Delta), \quad (16)$$

$$a_\mu^{\text{L}} = \int dt \omega(t) C(t) w^{\text{L}}(t), \quad w^{\text{L}}(t) \equiv \theta(t, t_1, \Delta). \quad (17)$$

with the $C(t)$ from the R -ratio. The extra weight functions $w^{\text{S,W,L}}$ pick the short, medium and long distance contributions of $C(t)$, respectively, and separate a_μ into three pieces. With typical parameters ($t_0 = 0.4$ fm, $t_1 = 1.0$ fm, $\Delta = 0.15$ fm), a_μ^{W} suppresses the contribution of $C(t)$ from $t \ll t_0$ and $t \gg t_1$, and can have smaller uncertainty using $C(t)$ from lattice QCD compared to that from the R -ratio. a_μ^{W} also provides a good reference to compare the independent lattice QCD results with good precision, in order to check the systematic uncertainties due to different lattice actions and their respective discretization errors.

We shall define the re-scaled connected light and strange quark contributions as

$$\bar{a}_{\text{con},l}^{\text{X}} = \bar{a}_{\text{con}}^{\text{X}}(m_l), \quad \bar{a}_{\text{con},s}^{\text{X}} = \frac{1}{5} \bar{a}_{\text{con}}^{\text{X}}(m_s),$$

$$\bar{a}_{\text{con}}^{\text{X}}(m_q) \equiv \frac{5}{9} \int dt w^{\text{X}}(t) \omega(t) C_f^{\text{con}}(t; m_q) \times 10^{10}, \quad (18)$$

where $X \in \{\text{S, W, L}\}$ and m_l and m_s are the physical light and strange quark masses, respectively. We use the local vector current in the calculation and apply the

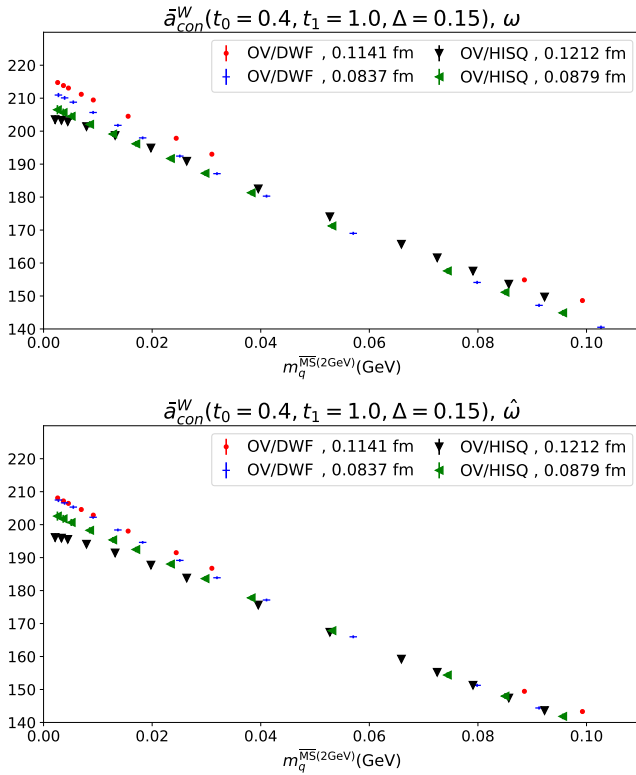


FIG. 2. The quark mass m_q dependence of the connected insertion contribution $\bar{a}_{\text{con}}^W(m_q)$ based on the original ω (defined in Eq. 5, upper panel) and the modified one ($\hat{\omega}$ as defined in Eq. 6, lower panel), on four ensembles we used.

axial-vector normalization constant Z_A obtained from PCAC [27] since the local vector current normalization constant obeys $Z_V = Z_A$ for the overlap fermion. As shown in Fig. 1, Z_A agrees with Z_V very well at the massless limit. (Z_V is determined from the forward matrix element $Z_V \equiv 2E/\langle\pi(p)|V_4|\pi(p)\rangle$ with $\vec{p} = 0$ in Ref. [28].) The uncertainty of Z_A is at the 0.01% level and can be ignored based on the precision target. Note that the last systematic uncertainty of the Z_A in Ref. [27] is not necessary here as we don't need to extrapolate the strange quark mass in the sea to the chiral limit.

Since the long distance contribution has been investigated in Ref. [8] and suppressing the statistical uncertainty using the bounding method can be non-trivial, we will concentrate on the medium-range contribution, \bar{a}_{con}^W , and the short-range one, \bar{a}_{con}^S , in this work. In Fig. 2, we show the result of $\bar{a}_{\text{con}}^W(m_q)$ on the four physical-point ensembles as a function of the quark mass renormalized to the $\overline{\text{MS}}$ scheme at 2 GeV through the RI/MOM method [27]. Compared to the values in the upper panel which use the original ω , those in the lower panel using the discretized $\hat{\omega}$ have smaller differences between ensembles except for the light quark mass region of the OV/HISQ case. It suggests that the modified definition might suppress the discretization error. But the m_q dependence in the small m_q region is non-linear and

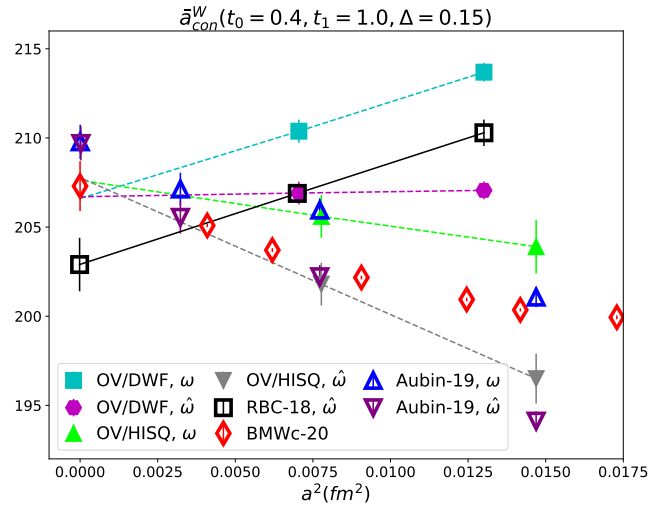


FIG. 3. The lattice spacing dependence of $\bar{a}_{\text{con},l}^W$ for different actions and weight functions are plotted with filled symbols. Results with unitary valence and sea actions, namely, RBC-18 [8] with DWF (black open boxes), Aubin-19 [13] with HISQ (blue and purple open triangles) and BMWc-20 [12] with a 4stout, staggered fermion action (red open diamonds), are also shown in the figure for comparison. The solid black line is the RBC extrapolation in a^2 with $\hat{\omega}$ [8]. The dashed lines are a^2 extrapolations of the mixed action results based only on two lattice spacings.

then the difference between the OV/HISQ result from the a12m130 and a09m130 ensembles is larger with $\hat{\omega}$ compared to that using ω .

By interpolating the partially quenched valence quark mass to the corresponding pion mass 135 MeV, we obtain the light quark contribution $\bar{a}_{\text{con},l}^W$ as shown in Fig. 3. We note that the modification of ω to $\hat{\omega}$ suppresses the discretization error in the OV/DWF setup (cyan and purple) but has the reversed effect on the OV/HISQ setup (green and gray). For comparison, we also show the results for unitary DWF [8] (open black box) and unitary HISQ [13] (open triangles). One can see that while those at larger lattice spacings have obvious differences, our results at $a \sim 0.08\text{--}0.09$ fm are consistent with the unitary results within uncertainty. Such a difference would be a discretization effect since it decreases with smaller lattice spacing. Thus, one expects that there will be no valence fermion action dependence at this and smaller lattice spacings. However, the OV/DWF and OV/HISQ results are conspicuously different at $a \sim 0.08\text{--}0.09$ fm. This is an indication that there is still sea dependence at this lattice spacing. After the linear a^2 continuum extrapolation, the OV/DWF result 206.7(1.5) and the OV/HISQ result 207.7(3.1), both using $\hat{\omega}$, are consistent with each other, and each is independent of using ω or $\hat{\omega}$. These results are consistent with the Budapest-Marseille-Wuppertal collaboration (BMWc) value 207.3(1.4) [12], but are a few σ larger than the RBC value 202.9(1.5) [8]. Since all the cases use linear a^2 continuum extrapolation,

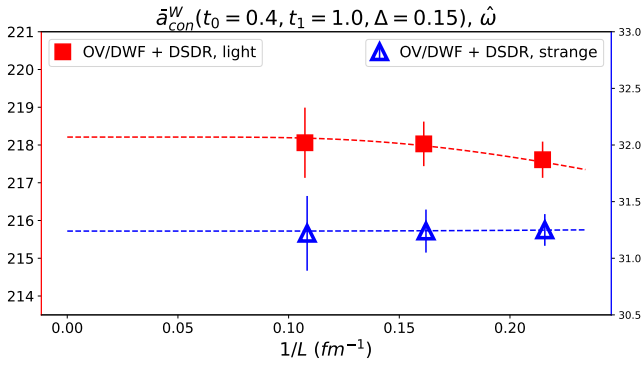


FIG. 4. The volume dependence of $\bar{a}_{\text{con},l}^W$ (red boxes and left y -axis) and $\bar{a}_{\text{con},s}^W$ (blue triangles and right y -axis) based on the DSDR ensembles at $a = 0.194$ fm. The $\bar{a}_{\text{con},l}^W$ values here are much larger than those in Fig. 3 due to the discretization errors.

it suggests that the $\mathcal{O}(a^4)$ effect is not negligible in a least one of these cases. We will elaborate on this point in the Summary and Discussion section.

One possible source of the OV/DWF-OV/HISQ discrepancy at $a \sim 0.08 - 0.09$ fm could be related to the gauge actions used in the DWF and HISQ ensembles, as different improvements make the bare gauge coupling in the RBC ensembles (2.13–2.25) and MILC ensembles (3.60–3.78) differ by a factor of ~ 1.7 . Such a possibility can be checked with HISQ+Iwasaki and DWF+Iwasaki simulations at $a = 0.08$ fm on a smaller lattice.

Since the volumes of the 4 ensembles are close to each other ($1/L \in [0.172, 0.184]$ fm^{-1}), we use the Mobius+Iwasaki+DSDR ensembles [16, 18] from the RBC/UKQCD collaboration to estimate the finite volume effect. As shown in Fig. 4, the finite volume effect with an empirical form $a + b \exp(-m_\pi L)$ for the case with $1/L \sim 0.18$ fm^{-1} is $-0.36(56)$ for the light quarks (red boxes, left y -axis) and $0.01(18)$ for the strange quark (blue triangles, right y -axis). They cannot explain the difference between our linear a^2 continuum extrapolated $\bar{a}_{\text{con},l}^W$ and the corresponding RBC value.

Combining the physical light quark mass $m_l^{\overline{\text{MS}}}(2 \text{ GeV}) = 3.74(9)$ MeV [29] via the RI/MOM scheme [27], and the ratio $m_s/m_l = 27.42(12)$ from the FLAG review [30], we can estimate the physical strange quark mass to be $m_s^{\overline{\text{MS}}}(2 \text{ GeV}) = 103(3)$ MeV. With this estimate, we show the strange quark contribution $\bar{a}_{\text{con},s}^W$ in Fig. 5. Similar to the light quark case, the linear a^2 extrapolated OV/DWF result of $26.7(3)$ and OV/HISQ result of $27.5(6)$ are consistent within the systematic uncertainty due to the strange quark mass (which is about 0.4). They are also consistent with the RBC value of $27.0(2)$ (open black box in the figure).

Next, we turn to the short distance contribution $\bar{a}_{\text{con},l/s}^S$, with the results shown in Fig. 6. We can see that the linear $\mathcal{O}(a^2)$ lines are almost the same on both the RBC and MILC ensembles for both the light and strange

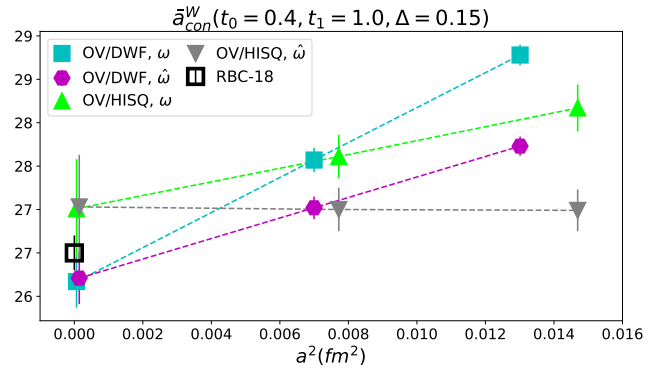


FIG. 5. The lattice spacing dependence of $\bar{a}_{\text{con},s}^W$. The DWF result extrapolated to the continuum limit [8] is also shown in the figure for comparison.

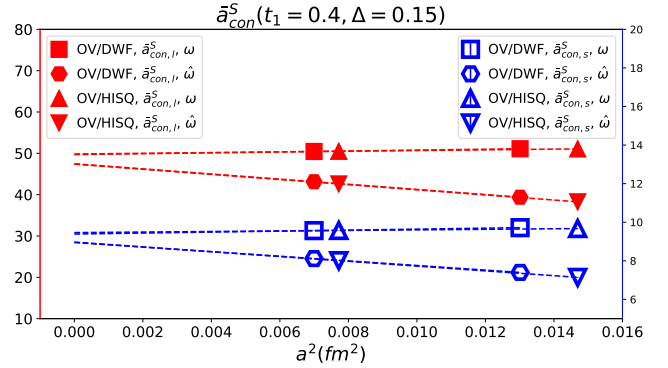


FIG. 6. The lattice spacing dependence of the short-distance contributions $\bar{a}_{\text{con},l}^S$ (red data points with the left y -axis) and $\bar{a}_{\text{con},s}^S$ (blue data points with the right y -axis), using either ω or $\hat{\omega}$. One can see that the action dependence almost vanishes and then is much weaker than that of the medium-distance contribution \bar{a}_{con}^W .

quark mass cases, and the linear a^2 continuum extrapolated values of the OV/DWF and OV/HISQ setups are consistent within the uncertainty (except for the case of $\bar{a}_{\text{con},s}^S$ using ω where the extrapolated values from the two setups differ by $0.07(2)$). But it is interesting that the discretization error of \bar{a}_{con}^S using ω is much smaller compared to that using $\hat{\omega}$, and the extrapolated values using the two definitions are separated by more than 5σ ($\sim 5\%$ difference) for both the light and strange quark cases.

This motivates us to repeat the calculation on the HISQ ensembles at a ~ 310 MeV pion mass with a larger lattice spacing range $a \in [0.04, 0.12]$ fm to check the lattice spacing dependence. Fig. 7 shows that the linear a^2 extrapolation still works well for $\bar{a}_{\text{con},l}^W$ (blue data points with the right y -axis), and using $\hat{\omega}$ can suppress the discretization error (similar to the OV/DWF results at the physical point). On the other hand, we can also see that $\bar{a}_{\text{con},l}^S$ (red data points with the left y -axis) is less sensitive to the lattice spacing when we use the original ω instead of $\hat{\omega}$, and the tension between the linear a^2 extrapolated

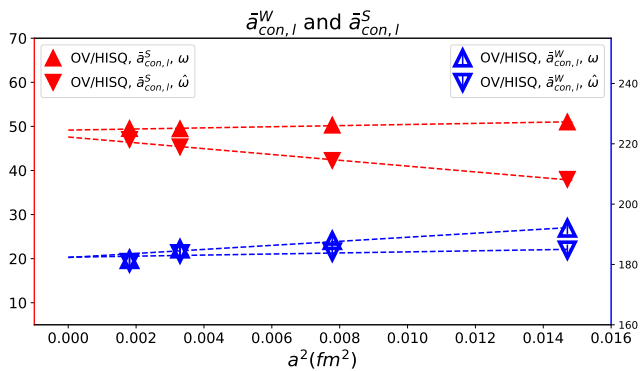


FIG. 7. The lattice spacing dependence of $\bar{a}_{\text{con},l}^S$ (red data points with the left y -axis) and $\bar{a}_{\text{con},l}^W$ (blue data points with the right y -axis) on HISQ ensembles with pion mass $m_\pi \simeq 310$ MeV, using either ω or $\hat{\omega}$.

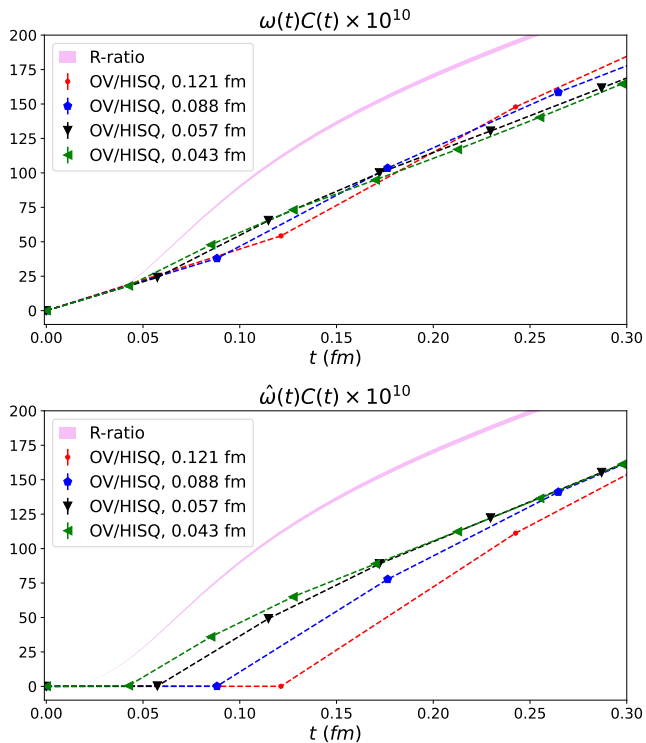


FIG. 8. The values of $\omega(t)C(t)$ (upper panel) and $\hat{\omega}(t)C(t)$ (lower panel) at the small t region with pion mass $m_\pi \simeq 310$ MeV.

values using either ω or $\hat{\omega}$ still exists. It suggests that using $\hat{\omega}$ introduces an extra discretization error in the small t region. Adding a^4 terms in the continuum extrapolation of $\bar{a}_{\text{con},l}^S$ using $\hat{\omega}$ can suppress the inconsistency.

$\bar{a}_{\text{con},l}^S$ corresponds to the integral of $\omega(t)C(t)$ in the small t region, and thus its discretization effect can be illustrated through the values of $\omega(t)C(t)$ (Fig. 8, upper panel) and those of $\hat{\omega}(t)C(t)$ (lower panel). The definition of $\hat{\omega}$ forces $\hat{\omega}(a) \propto a^2$, and, as a consequence, the integral of $\hat{\omega}(t)C(t)$ has a sizable discretization error

around $t \sim 1a$ [8]. This is illustrated in the lower panel of Fig. 8. Since $\hat{\omega}(t)C(t)$ is not linear in t in the range of $t \in [0.0, 0.2]$ fm, the extra $\mathcal{O}(a^4)$ effect is not avoidable and cannot be mocked up with a linear a^2 continuum extrapolation.

Fig. 8 also shows the values of $\omega(t)C(t)$ (pink band), with $C(t) = 1/(12\pi^2) \int_0^\infty d(\sqrt{s})R(s)se^{-\sqrt{s}t}$ from [14], using the most recent analysis of the R -ratio data [6]. The pink band is about 40% higher than the connected light quark contribution at $t \sim 0.2$ fm, it should be primarily due to the connected strange and charm contributions and is worth further investigation in the future.

IV. SUMMARY AND DISCUSSION

In this work, we calculated the light and strange contribution of a_μ from the connected vector correlators in the medium window ($t_0 = 0.4$ fm, $t_1 = 1.0$ fm, $\Delta = 0.15$ fm) using the overlap fermion, on the physical point ensembles using either DWF+Iwasaki (at $a = 0.084/0.114$ fm) or HISQ+Symanzik (at $a = 0.088/0.121$ fm) configurations. Our linear a^2 extrapolated $\bar{a}_{\text{con},s}^W$ result is 26.7(3) using the OV/DWF setup; it is consistent with the value 27.5(6) using the OV/HISQ setup and also with the unitary DWF value from RBC [8].

For $\bar{a}_{\text{con},l}^W$, the mixed action results on the ensembles with $a < 0.1$ fm are consistent with the unitary DWF or HISQ calculations, but those at $a > 0.1$ fm are different from their respective unitary results by many sigmas. After linear a^2 continuum extrapolations, the OV/DWF result 206.7(1.5) and OV/HISQ result 207.7(3.1) are consistent with each other and also with the BMWc value 207.3(1.4) [12]. But these are a few σ larger than the unitary DWF value 202.9(1.5) [8]. It suggests that the $\mathcal{O}(a^4)$ effect should be important in certain lattice setups.

Note that if the upcoming RBC result on a 96^3 lattice at $a \sim 0.07$ fm [31] turns out to lie on the black line of Fig. 3, it would be a strong indication that the $\mathcal{O}(a^4)$ contribution is small for unitary DWF and that the mixed OV/DWF and OV/HISQ results could each have a sizable $\mathcal{O}(a^4)$ correction. Such $\mathcal{O}(a^4)$ behaviors in OV/DWF and OV/HISQ have been observed in Δ_{mix} , a low-energy constant used to measure the mixed action effect in the pion mass in LO chiral perturbation theory [29, 32].

We also calculated the short range contribution and predict $\bar{a}_{\text{con},l+s}^S = 57.8(0.1)(1.5)$ with the systematic error estimated from half of the difference between the predictions of the results from ω and $\hat{\omega}$. Even though using $\hat{\omega}$ introduces an extra discretization error, it is not a big issue after linear a^2 continuum extrapolation. It would be valuable to verify our observation on other lattice setups.

Since the tension among the \bar{a}_{con}^W and \bar{a}_{con}^S values using different kinds of lattice setups is much smaller than that between a_μ^{HVP} from the R -ratio and that inferred from the Fermilab experiment, we expect that the $\mathcal{O}(a^4)$ effect

is more important in the long-distance contribution \bar{a}^L , and should be examined carefully. We also suggest a unitary HISQ+Iwasaki simulation at around $a = 0.09$ fm to test the gauge action dependence.

ACKNOWLEDGMENTS

We thank the RBC/UKQCD, and MILC collaborations for providing us their gauge configurations, A. Keshavarzi for sharing their R -ratio data, and F. He, C. Lehner and L. Lellouch for valuable inputs and discussion. K.L. thanks T. Blum and A. El-Khadra for informative discussions. Most of the production was performed using the the GWU code [33, 34] through the HIP programming model [35], and the data analysis was based on the Qlattice package. This work is supported in part by the U.S. DOE Grant No. DE-SC0013065 and DOE Grant No. DE-AC05-06OR23177 which is within the framework of the TMD Topical Collaboration. This publication received funding from the French National Research

Agency under the contract ANR-20-CE31-0016. Y.Y. is supported in part by a NSFC-DFG joint grant under Grant No. 12061131006 and SCHA 458/22 and also the Strategic Priority Research Program of Chinese Academy of Sciences, Grant No. XDC01040100, XDB34030303 and XDPB15. The numerical calculation were carried out on the SunRising-1 computing platform, and HPC Cluster of ITP-CAS. This research used resources of the Oak Ridge Leadership Computing Facility at the Oak Ridge National Laboratory, which is supported by the Office of Science of the U.S. Department of Energy under Contract No. DE-AC05-00OR22725. This work used Stampede time under the Extreme Science and Engineering Discovery Environment (XSEDE), which is supported by National Science Foundation Grant No. ACI-1053575. We also thank the National Energy Research Scientific Computing Center (NERSC) for providing HPC resources that have contributed to the research results reported within this paper. We acknowledge the facilities of the USQCD Collaboration used for this research in part, which are funded by the Office of Science of the U.S. Department of Energy.

-
- [1] B. Abi *et al.* (Muon $g-2$), Phys. Rev. Lett. **126**, 141801 (2021), arXiv:2104.03281 [hep-ex].
 - [2] T. Albahri *et al.* (Muon $g-2$), Phys. Rev. D **103**, 072002 (2021), arXiv:2104.03247 [hep-ex].
 - [3] G. W. Bennett *et al.* (Muon $g-2$), Phys. Rev. D **73**, 072003 (2006), arXiv:hep-ex/0602035.
 - [4] T. Aoyama *et al.*, Phys. Rept. **887**, 1 (2020), arXiv:2006.04822 [hep-ph].
 - [5] M. Davier, A. Hoecker, B. Malaescu, and Z. Zhang, Eur. Phys. J. C **80**, 241 (2020), [Erratum: Eur.Phys.J.C 80, 410 (2020)], arXiv:1908.00921 [hep-ph].
 - [6] A. Keshavarzi, D. Nomura, and T. Teubner, Phys. Rev. D **101**, 014029 (2020), arXiv:1911.00367 [hep-ph].
 - [7] S. Borsanyi *et al.* (Budapest-Marseille-Wuppertal), Phys. Rev. Lett. **121**, 022002 (2018), arXiv:1711.04980 [hep-lat].
 - [8] T. Blum, P. A. Boyle, V. Gülpers, T. Izubuchi, L. Jin, C. Jung, A. Jüttner, C. Lehner, A. Portelli, and J. T. Tsang (RBC, UKQCD), Phys. Rev. Lett. **121**, 022003 (2018), arXiv:1801.07224 [hep-lat].
 - [9] A. Gérardin, M. Cè, G. von Hippel, B. Hörz, H. B. Meyer, D. Mohler, K. Ottnad, J. Wilhelm, and H. Wittig, Phys. Rev. D **100**, 014510 (2019), arXiv:1904.03120 [hep-lat].
 - [10] C. T. H. Davies *et al.* (Fermilab Lattice, LATTICE-HPQCD, MILC), Phys. Rev. D **101**, 034512 (2020), arXiv:1902.04223 [hep-lat].
 - [11] D. Giusti, V. Lubicz, G. Martinelli, F. Sanfilippo, and S. Simula, Phys. Rev. D **99**, 114502 (2019), arXiv:1901.10462 [hep-lat].
 - [12] S. Borsanyi *et al.*, Nature **593**, 51 (2021), arXiv:2002.12347 [hep-lat].
 - [13] C. Aubin, T. Blum, C. Tu, M. Golterman, C. Jung, and S. Peris, Phys. Rev. D **101**, 014503 (2020), arXiv:1905.09307 [hep-lat].
 - [14] D. Bernecker and H. B. Meyer, Eur. Phys. J. A **47**, 148 (2011), arXiv:1107.4388 [hep-lat].
 - [15] C. Lehner and T. Izubuchi, PoS **LATTICE2014**, 164 (2015), arXiv:1503.04395 [hep-lat].
 - [16] R. Arthur *et al.* (RBC, UKQCD), Phys. Rev. D **87**, 094514 (2013), arXiv:1208.4412 [hep-lat].
 - [17] T. Blum *et al.* (RBC, UKQCD), Phys. Rev. **D93**, 074505 (2016), arXiv:1411.7017 [hep-lat].
 - [18] P. Boyle *et al.*, Phys. Rev. D **93**, 054502 (2016), arXiv:1511.01950 [hep-lat].
 - [19] A. Bazavov *et al.* (MILC), Phys. Rev. D **87**, 054505 (2013), arXiv:1212.4768 [hep-lat].
 - [20] T.-W. Chiu, Phys. Rev. **D60**, 034503 (1999), arXiv:hep-lat/9810052 [hep-lat].
 - [21] K.-F. Liu, Int. J. Mod. Phys. **A20**, 7241 (2005), arXiv:hep-lat/0206002 [hep-lat].
 - [22] P. H. Ginsparg and K. G. Wilson, Phys. Rev. **D25**, 2649 (1982).
 - [23] E. Follana, Q. Mason, C. Davies, K. Hornbostel, G. P. Lepage, J. Shigemitsu, H. Trotter, and K. Wong (HPQCD, UKQCD), Phys. Rev. D **75**, 054502 (2007), arXiv:hep-lat/0610092.
 - [24] A. Li *et al.* (xQCD), Phys. Rev. D **82**, 114501 (2010), arXiv:1005.5424 [hep-lat].
 - [25] M. Gong *et al.* (XQCD), Phys. Rev. D **88**, 014503 (2013), arXiv:1304.1194 [hep-ph].
 - [26] K. Zhang, Y.-Y. Li, Y.-K. Huo, A. Schäfer, P. Sun, and Y.-B. Yang (χ QCD), Phys. Rev. D **104**, 074501 (2021), arXiv:2012.05448 [hep-lat].
 - [27] F. He and Y.-B. Yang, in *38th International Symposium on Lattice Field Theory* (2021) arXiv:2112.03532 [hep-lat].
 - [28] G. Wang, J. Liang, T. Draper, K.-F. Liu, and Y.-B. Yang (χ QCD), Phys. Rev. D **104**, 074502 (2021), arXiv:2006.05431 [hep-ph].

- [29] D.-J. Zhao and Y.-B. Yang (xQCD), (2022), arXiv:2201.04910 [hep-lat].
- [30] S. Aoki *et al.* (Flavour Lattice Averaging Group), *Eur. Phys. J. C* **80**, 113 (2020), arXiv:1902.08191 [hep-lat].
- [31] T. Blum, private communication.
- [32] D. Zhao *et al.*, in preparation.
- [33] A. Alexandru, C. Pelissier, B. Gamari, and F. Lee, *J. Comput. Phys.* **231**, 1866 (2012), arXiv:1103.5103 [hep-lat].
- [34] A. Alexandru, M. Lujan, C. Pelissier, B. Gamari, and F. X. Lee, in *Proceedings, 2011 Symposium on Application Accelerators in High-Performance Computing (SAAHPC'11): Knoxville, Tennessee, July 19-20, 2011* (2011) pp. 123–130, arXiv:1106.4964 [hep-lat].
- [35] Y.-J. Bi, Y. Xiao, W.-Y. Guo, M. Gong, P. Sun, S. Xu, and Y.-B. Yang, *Proceedings, 37th International Symposium on Lattice Field Theory (Lattice 2019): Wuhan, China, June 16-22 2019*, PoS **LATTICE2019**, 286 (2020), arXiv:2001.05706 [hep-lat].